

## **Acoustic reflections in the water column of Krishna-Godavari offshore basin, Bay of Bengal**

Satish K. Sinha <sup>a</sup>; Pawan Dewangan <sup>b</sup>; Kalachand Sain <sup>c</sup>

<sup>a</sup> Rajiv Gandhi Institute of Petroleum Technology, Rae Bareli, INDIA 229316

<sup>b</sup> CSIR-National Institute of Oceanography, Goa, INDIA

<sup>c</sup> CSIR-National Geophysical Research Institute, Hyderabad, INDIA

Corresponding author: E-mail: [ssinha@rgipt.ac.in](mailto:ssinha@rgipt.ac.in) , [satish.sinha@gmail.com](mailto:satish.sinha@gmail.com)

### **Abstract**

Seismic oceanographic studies from various oceans worldwide have indicated that the acoustic reflections are mostly observed along thermal boundaries within the water column. However, we present a case study of seismic data from Krishna-Godavari Basin which shows that salinity variations also play an important role in the occurrence of water column reflections. The observed reflection is modeled using the reflectivity series derived from the salinity and temperature profiles from a nearby CTD location. Sensitivity analysis of temperature and salinity on soundspeed shows that the effect of salinity cannot be ignored for modeling acoustic reflections. The synthetic seismogram matches well with the observed reflection seismic data. Remarkable similarities between the reflection seismic and the salinity profile in the upper thermocline suggest that the importance of salinity variations on the water column reflection. Furthermore, impedance inversion of the reflectivity data reveals several thermohaline structures in the water column. The origin of these thermohaline structures is largely unaddressed and may be attributed to the fresh water influx coming from Himalayan and Peninsular rivers or due the presence of different water masses in the Indian Ocean which warrants detailed study using concurrent seismic and CTD data.

**Keywords:** Seismic oceanography, reflectivity series, seismic modeling, ‘colored’ inversion, thermohaline structures

## I. INTRODUCTION

Acoustic reflections within water column have been reported worldwide. These reflections are manifestations of acoustic impedance contrasts produced by fine scale thermohaline structures. They represent the variability in temperature and salinity in tropics and subtropics regions. In a pioneering work, Holbrook, *et al.* <sup>1</sup> showed a seismic reflection between the Labrador Current and the North Atlantic Current, and attributed the occurrence of seismic reflection to the change in temperature. Further, they argued that temperature had dominant influence on soundspeed in the uppermost 400 m of the ocean. Worcester, *et al.* <sup>2</sup> used the arrival times of acoustic signals to invert for temperature which is now constitute the field of oceanic thermometry. Any deviation in modeled arrival time is largely attributed to change in temperature. The full waveform inversion of multichannel seismic (MCS) data was used to produce temperature profile in the Norwegian sea assuming a constant salinity <sup>3</sup>. Similarly, the MCS data from southwest of Iberian Peninsula are inverted for both temperature and salinity <sup>4</sup> and verified using the simultaneously acquired XBT (eXpendable Bathy Thermograph) and CTD (Conductivity-Temperature-Depth) data. Worldwide, the primary cause of acoustic reflections in the water column is assumed to be from the change in temperature, but the impedance contrast can also be produced by the change in salinity. We are not aware of any work which models the impedance contrast using the changes in both temperature and salinity. However, the temperature and salinity gradients have been used in generating synthetic seismograms and are compared with the reflection seismic data<sup>5-7</sup>.

In order to model the impedance contrast across different layers, known as reflectivity series, depth-wise variation in soundspeed and density of seawater are required. Theoretical formulation exists for soundspeed which is closely linked with the equation of state in sea water. It considers the process of propagation of wave in compressible fluid as an adiabatic process. The well known Matthews and Kuwahara tables<sup>8,9</sup> are based on theoretical formulations. However, it produces inaccurate results for seawater temperature and salinity ranges. In order to overcome this difficulty, several empirical relationships are established to estimate soundspeed from temperature, salinity and depth (pressure) data<sup>10-15</sup>. In the present study, Coppens' equation is used to derive soundspeed from CTD data. Similar to the soundspeed, the density of sea water is also a function of salinity, temperature and pressure <sup>16-18</sup> which can be estimated using empirical relationship. The empirical equation given by Fofonoff <sup>19</sup> fitted the measured densities with a standard deviation of 0.0036 kg/m<sup>3</sup> at atmospheric pressure and 0.009 kg/m<sup>3</sup> over the oceanic pressure range. Millero and Poisson <sup>20</sup> used the same density data, published in Millero, *et al.* <sup>21</sup> and Poisson, *et al.* <sup>22</sup>, to determine an equation of state for

seawater at 1-atm. The equations are recommended by the UNESCO (United Nations Educational, Scientific and Cultural Organization) joint panel on oceanographic tables and standards.

In the present study, density and soundspeed profiles are estimated using the parameters derived from a CTD profile in the study area. The reflectivity series is computed from the acoustic impedance and a convolution-based forward modeling is used to generate the synthetic seismogram assuming a known source wavelet<sup>23</sup>. The synthetic seismograms are compared with the available MCS data to understand the effect of density and soundspeed variations on the acoustic reflections. The effect of salinity variation is highlighted by generating the synthetic seismogram using a smoothed temperature profile (a higher order curve fitting to the original temperature profile) while keeping the salinity unchanged. Likewise, the effect of temperature variation is highlighted using a smoothed salinity profile. Further, the MCS data are inverted for impedances contrast across different layers representing thermohaline structures in the water column using seismic ‘colored’ inversion, an effective tool used in oil and gas exploration<sup>24</sup>.

## **II. STUDY AREA AND DATA AVAILABLE**

The study area is located in the offshore Krishna-Godavari (K-G) Basin, along the eastern continental margin of India (Fig. 1). Multi-channel seismic (MCS) data were acquired during the first week of May 2004, by Oil and Natural Gas Commission (ONGC) for gas hydrate exploration<sup>25</sup> in the K-G basin. Eight 40 cu.in. airgun were used at the seismic source which were fired at every 12.5m . A 1.5 km long streamer with 120 channels at an interval of 12.5 m was used to receive the seismic signal. The near offset distance (i.e. distance between the airgun and the first hydrophone of the streamer) is 70m. The data were recorded with a 1 ms sampling rate after applying a high cut filter of 500 Hz.

The seismic survey was not designed for oceanographic studies and therefore, no CTD data was acquired in the study area during the acquisition of seismic data. The nearest CTD data available is about 2 km away from Line 1 (Fig. 1) that was recorded in the middle of January, 2004. While there is a gap of 4-5 months between the acquisition of CTD profile and seismic data, the analysis of climatology data suggests that there is no appreciable change in the CTD profiles below the depth of ~50m of water depth during this period in the Bay of Bengal<sup>26,27</sup>. A Sea Bird Electronics (SBE) 911 Plus system was used by National Institute of Oceanography (CSIR-NIO) to acquire CTD data under Gas Hydrate program. The observed temperature and salinity profiles from the CTD data (Fig. 2) are used to estimate the soundspeed and density profiles which in turn are used for reflectivity modeling to generate the synthetic seismogram.

### III. THEORY AND METHOD

#### A. Estimation of soundspeed in sea water

Soundspeed of seawater varies with temperature (T), salinity (S) and depth (D) (or, pressure). Several empirical relationships exist representing soundspeed (c) as a function of T, S, and D<sup>10-14, 28</sup>. In the present study, Coppens' equation (Eq. 1) is used for its simplicity and large range of temperatures over which it is valid.

$$\begin{aligned}
 c(T, D, S) = & c(T, 0, S) + [1.6 \times 10^{-6} + 2 \times 10^{-8}(S - 35)](S - 35)TD + (1.623 \times 10^{-2} \\
 & + 2.53 \times 10^{-5} T)D + (2.13 \times 10^{-7} - 1 \times 10^{-8} T)D^2 \\
 & \hspace{15em} (1) \\
 c(T, 0, S) = & 1449.05 + 4.57 T - 5.21 \times 10^{-2} T^2 + 2.3 \times 10^{-4} T^3 + (1.333 \\
 & - 1.26 \times 10^{-2} T + 9 \times 10^{-5} T^2)(S - 35)
 \end{aligned}$$

In Eq. (1), the temperature is expressed in degrees Celsius, salinity is in PSU, depth is in meters, and soundspeed is in m/s. Variation of soundspeed with depth computed using the observed temperature and salinity profiles is shown in Fig. 3a.

In order to understand the effect of T and S variations on soundspeed, sensitivity analysis is performed by differentiating Eq. 1 with respect to T and S.

$$\begin{aligned}
 \frac{dc}{dT} = & 4.57 - 1.26 \times 10^{-2}(S - 35) + [2.53 \times 10^{-5} + 1.6 \times 10^{-6}(S - 35) \\
 & + 2 \times 10^{-8}(S - 35)^2]D - 1 \times 10^{-8}D^2 - (0.1042 - 1.8 \times 10^{-4}(S - 35))T \\
 & + 6.9 \times 10^{-4} T^2 \hspace{10em} (2)
 \end{aligned}$$

$$\frac{dc}{dS} = 1.333 - [1.26 \times 10^{-2} - 1.6 \times 10^{-6}D - 4 \times 10^{-8}(S - 35)D]T + 9 \times 10^{-5} T^2 \quad (3)$$

Assuming a temperature of 22.3°C and salinity of 34.75 PSU at a depth of 100 m,  $\frac{dc}{dT}$  and  $\frac{dc}{dS}$  are computed to be 2.6 and 1.1, respectively. Soundspeed is more than twice as sensitive to temperature as compared to salinity<sup>29</sup>. The effect of salinity, however, cannot be ignored if the variation in salinity is significant as observed in the study area. Furthermore, sensitivity to salinity increases with increase in temperature (Fig. 4). In the open seas below the mixed layer (~50m water depth), temperatures are usually high and significant salinity variation are observed. In such regions, salinity effect on impedance and its reflection generating potential cannot be ignored.

## B. Estimation of density of sea water

Sea water density varies with temperature and salinity. Usually, it ranges between 1.02 gm/cc to 1.03 gm/cc. The empirical relationship by Millero and Poisson<sup>20</sup> is used to calculate sea water density from observed salinity (S) and temperature (T) profiles.

$$\rho = \rho_0 + AS + BS^{1.5} + CS^2, \quad (4)$$

where  $\rho_0$  represents the density of pure water in kg/m<sup>3</sup> and varies with temperature. The coefficients A and B are also functions of temperature and C is a constant. Salinity is expressed in PSU and temperature is in degree Celsius. The density of pure water<sup>30</sup> and the coefficients in Eq. 4 are given as<sup>20</sup>:

$$\rho_0 = 999.842594 + 6.793952 \times 10^{-2}T - 9.095290 \times 10^{-3}T^2 + 1.001685 \times 10^{-4}T^3 - 1.120083 \times 10^{-6}T^4 + 6.536332 \times 10^{-9}T^5, \quad (5)$$

$$A = 8.24493 \times 10^{-1} - 4.0899 \times 10^{-3}T + 7.6438 \times 10^{-5}T^2 - 8.2467 \times 10^{-7}T^3 + 5.3875 \times 10^{-9}T^4, \quad (6)$$

$$B = -5.72466 \times 10^{-3} + 1.0227 \times 10^{-4}T - 1.6546 \times 10^{-6}T^2, \quad (7)$$

$$C = 4.8314 \times 10^{-4}, \quad (8)$$

Estimated density profile from the CTD data is shown in Fig. 3b.

## C. Impedance, Reflectivity and Synthetic Seismogram

As sound wave travels through sea water column, it refracts and reflects from layers of different acoustic impedances. This layer property (i.e. acoustic impedance,  $AI$ ) is calculated by multiplying density with soundspeed,  $AI = \rho \times c$ . The density and soundspeed in seawater were calculated from the observed temperature and salinity profiles at the CTD location. The amplitude of reflected sound waves from different impedance layers is directly proportional to the reflection coefficient or reflectivity, determined by the impedance contrast between the two layers. For an incident normal sound wave, reflection coefficient is expressed as:

$$R = \frac{(AI_1 - AI_0)}{(AI_1 + AI_0)}, \quad (9)$$

where the subscripts refer to the layer ‘0’ and ‘1’, respectively. The reflectivity series computed for the CTD location is shown in Fig. 3c.

A one dimensional synthetic seismogram is generated by convolving reflectivity series with a source wavelet<sup>23</sup>. A Ricker wavelet with a peak frequency of 45 Hz is used as a source wavelet. The workflow for modeling synthetic seismogram is shown in Fig. 5. The synthetic seismogram produced for the CTD location is shown in Fig. 6 as an overlay (shown as wiggle traces) on the seismic section nearest to the CTD location. The distance between synthetic seismogram and seismic line is about 2 km. An overlay of salinity profile on the synthetic seismogram (Fig. 6) shows good correlation with the observed reflections. Furthermore, the synthetic seismograms are generated to highlight the effects of salinity variations on acoustic reflections (Fig. 7a), using smoothed temperature profile. Likewise, the effect of temperature variation only on acoustic reflection is highlighted (Fig. 7b) by using a smoothed salinity profile.

#### **D. Seismic ‘Colored’ Inversion**

The ‘colored’ inversion<sup>24</sup> is a process to match the average spectrum of inverted seismic data with the average spectrum of impedance. In this procedure, a single optimal matching filter is designed by cross-matching impedance data with the seismic reflection data. Acoustic impedance (AI) profile is computed from the estimated soundspeed and density. AI spectra invariably show ‘colored’ behavior as the earth naturally filters the higher frequencies. A smoothed curve-fit to the AI spectrum is used to design the inversion operator by matching it with the seismic spectra and rotating the phase by  $-90^\circ$ . Inversion result of the seismic data near the CTD location is shown in Fig. 8. Also, relative acoustic impedance derived from the CTD data is overlain on the seismic inversion result nearest to the location.

#### **E. Seismic Data Processing**

The seismic data was acquired with conventional acquisition design used in petroleum exploration. In such cases, any reflection amplitude in the water column are feeble compared to sea floor reflection and beneath<sup>31</sup>, and therefore, are susceptible to noise from various sources like ocean dynamics / unstable seas. Furthermore, in marine seismic data acquisition, acoustic signal propagating in the water column attenuates primarily due to geometrical spreading. Increasing gain may help visualize the water column reflections, however, noise will also be boosted along with the signal. We have used spectral balancing technique combined with de-noising based on wavelet transform<sup>32,33</sup>. Scale based de-noising bring out signal from weak reflectivity. Spectral balancing is essentially done in continuous wavelet transform (CWT) domain by modifying the scalogram and

then applying inverse transform to the select scales. The attenuation filter used in the modification of scalogram is derived by appropriately smoothing the scalogram.

Processing of the seismic data is achieved in the pre-stack domain. Broadening of bandwidth helped in precise picking of direct arrivals which in-turn help in shot stack corrections. Data is CDP (common-depth point) sorted before stacking. Distance between two CDPs is 6.25 m and the nearest offset is 70m. Time section is converted to depth using time-depth chart derived from soundspeed profile of CTD data. The two seismic lines (Fig. 1) were processed for the water column reflections are shown in Fig. 9. The combined seismic section joined at the intersection is shown in Fig. 10.

#### **IV. RESULTS AND DISCUSSION**

Generating synthetic seismogram from sonic and density logs is a common practice in hydrocarbon exploration, and it helps in understanding the observed reflections in seismic data. In the present study, a workflow is created to generate synthetic seismogram from the observed temperature and salinity profiles (Fig. 5). The established empirical relationships are used to compute soundspeed and density from temperature and salinity data which are in turn used to generate impedance (reflectivity) log (Fig. 3). The impedance log is convolved with Ricker wavelet to produce synthetic seismogram (Fig. 6). An excellent correlation is observed between the synthetic seismogram and seismic reflections (Fig. 6) in spite of the fact that the CTD location is about 2 km away from the seismic line#1 and differences in the acquisition time between the CTD and seismic data. The seismic profiles are converted to depth using the velocity estimated from CTD and are shown in Fig. 9. Most of the strong reflectors (i.e. thermohaline structures) are confined to a depth of about 300 meters. Interestingly, no shallow reflections are observed in the seismic data in water depth less than 50 m; in contrast strong reflections are observed in the synthetic seismogram from the CTD data due to impedance contrast between the shallow mixed layer (5 – 10 m) and halocline (10 – 50 m). We attributed this mismatch to the difference in the acquisition time between the seismic and CTD data. The CTD data was acquired in the month of January towards the end of winter monsoon and seismic data was acquired during the month of May before the onset of summer monsoon. Due to huge influx of fresh water from Krishna and Godavari rivers and large precipitation due to winter monsoon, shallow mixed layer is expected in the month of January which may explain strong reflectivity as observed on the synthetic seismogram (wiggle display in Fig. 6). In contrast, deeper mixed layer may be expected before the onset of summer monsoon due to mixing and hence, it would yield low impedance contrast in the shallow waters. This partly explains the absence of acoustic reflections in shallow water depth (<50m). In addition, conventional geometry for MCS data acquisition limits our ability to image very shallow reflections. The minimum offset (distance between the airgun and the

first hydrophone in the streamer cable) is about 70 m and the dominant frequency of source is 45 Hz. As a result, reflections shallower than 35 m will be difficult to image due to the interference with the direct arrivals. However, direct wave can be inverted for sea surface temperature<sup>34</sup>. In case of seismic analyses of water column reflections, the thermohaline features in the intermediate depths (i.e. ~50 to 300 m) and deeper water are of significance.

Seismic tie between two intersecting lines indicates performance of seismic data processing. Two mutually perpendicular seismic lines (Line#1 and Line#2) processed independently are shown in Fig. 9 and are tied at the intersection (Fig. 10). This is an impressive seismic tie for 2D lines given high frequency content, short time-arrivals and feathering of hydrophone cables during data acquisition. A gentle dipping water column reflection towards SE is observed in Line 2 (Fig. 9) suggesting the deepening of the thermocline structures.

Reflection observed on seismic sections represents the variation in acoustic impedance. As shown in Fig. 5, the impedance variation of seawater depends on both temperature and salinity profiles. Several studies in seismic oceanography have considered only temperature variations, and shows good correlation between the water column reflections and the change in temperature gradient<sup>3, 5, 35, 36</sup>. However, we present a case study area that shows the importance of salinity variation in the coastal region of Bay of Bengal (BoB) which receives large influx of freshwater from Himalayan and Peninsular Rivers of the Indian sub-continent. Therefore, the effect of salinity cannot be ignored in seismic oceanography. The study of water column using seismic reflection technique has a limitation on imaging depth largely due to the acquisition geometry. The reflection shallower than 35m may represent the base of the mixed layer or halocline (~50 m thick) cannot be imaged from this technique. However, salinity variation in the intermediate depth in the upper thermocline can be resolved from this technique. Any stratification in that zone is likely to remain least affected by the seasonal variation in water influx and can be studied from this technique. The sensitivity analysis of temperature and salinity on soundspeed shows that the effect of salinity variation is not negligible. With increasing temperature, sensitivity of soundspeed to salinity also increases (Fig. 4). Salinity profile is overlain on synthetic seismogram (Fig. 6) to show very good correlation between salinity variations and seismic reflections indicating the influence of salinity on seismic reflection. Furthermore, the effect of salinity is highlighted from modeling studies as shown in Fig. 7a. The decrease in amplitude of synthetic seismogram below 175 m depth indicates reduced salinity variation with depth. Likewise, the effect of temperature is highlighted in Fig. 7b. The acoustic reflections are dominantly controlled by temperature variations for water depth below 200 m. Thus,



interpretation of thermohaline structures in the intermediate water depth (Fig. 8) must consider salinity variation in addition to the temperature variations.

Seismic data is commonly inverted for impedance to trace bodies of similar impedances. In seismic oceanography, these impedance layers are essentially thermohaline structures. Seismic ‘colored’ inversion uses impedance log data to invert for reflectivity data <sup>24</sup>. Long wavelength variation is filtered from impedance log to give relative acoustic impedance (RAI) curve (Fig. 8). An excellent correlation is observed between the impedance estimated from the nearest seismic location and that estimated from the CTD data. The result from the impedance inversion for the full seismic profile (NW-SE line) is shown in Fig. 11. Considering dominant frequency of 45 Hz for the source, vertical resolution of seismic data would be about 8 meters (i.e. quarter of a wavelength). The ‘colored’ inversion process further boosts the frequency content, thereby increasing the vertical resolution to ~6 meters. Alternating layers of high and low RAI thermohaline structures show pattern similar to sedimentary structures and have general dip in SE direction. The layer represented with a dashed line has a slope of 0.35 degrees possibly suggesting the deepening of thermocline but concurrent and denser CTD measurements are required to understand the origin of this dipping layer. By observing the color range for impedance, a general pattern emerges from Fig. 11. In the upper part, impedance range is higher than the lower part. These low impedance layers are likely due to lower salinity variations.

The Bay of Bengal (BoB) is traditionally considered to be a region of lesser biological productivity and has been supported by various biological and isotopic studies <sup>37-39</sup>. It has been suggested that strong stratification in BoB inhibits migration of nutrients upward; however, the physical processes causing such stratification are largely unaddressed. Such stratified layers (or thermohaline structures) in the intermediate and deeper waters can be imaged using seismic reflection method. The present study is limited by the fact that seismic and CTD were not acquired simultaneously and the objectives of seismic studies were different. Future research in the area may be planned so that simultaneous acquisition of salinity and temperature profiles in addition to the seismic reflection data can be achieved.

## V. CONCLUSIONS

In the present study, thermohaline structures are studied in Krishna-Godavari Basin using the available multi-channel seismic data. After special processing of seismic data using wavelet transform based spectral balancing and de-noising, several acoustic reflections in the intermediate water depth are observed in the seismic data representing thermohaline structure in the water column of K-G basin. These thermohaline structures are formed due to impedance contrast in the water

column resulting from temperature and salinity variation. The effect of temperature and salinity on the soundspeed is studied using sensitivity analysis, and it showed that the effect of temperature is more than twice as compared to salinity. However, the effect of salinity is more pronounced with higher temperatures, and cannot be ignored if the salinity variation is significant as observed in the study area. The generation of synthetic data using the available CTD information showed good correlation with the seismic data confirming the effect of both temperature and salinity on the acoustic impedance. The modeling of salinity and temperature effects shows that salinity variations are more pronounced in the upper thermocline between 100 and 175 m whereas temperature variations are more pronounced below 200 m water depth. Seismic ‘colored’ inversion is used to estimate the impedance contrast of the seismic data after calibrating with the available CTD data. Several thermohaline structures are observed in the seismic data which have a general dip in SE direction.

## **Acknowledgements**

We would like to thank the directors of CSIR-NGRI, CSIR-NIO and RGIPT for supporting this study. We thank K. Vishwanath and B.J.P Kumar, DGH for providing the seismic data used in the present study. The authors acknowledge the Indian Oceanographic Data Center (IODC), CSIR-NIO for providing the CTD data. The work was performed at RGIPT under research collaboration with CSIR-NGRI and CSIR-NIO. This is CSIR-NIO contribution no \_\_\_\_.

## **REFERENCES**

- <sup>1</sup> W. S. Holbrook, P. Paramo, S. Pearse and R. W. Schmitt, "Thermohaline fine structure in an oceanographic front from seismic reflection profiling," *Science* **301**, 821-824 (2003).
- <sup>2</sup> P. F. Worcester, B. D. Cornuelle, M. A. Dzieciuch, W. H. Munk, B. M. Howe, J. A. Mercer, R. C. Spindel, J. A. Colosi, K. Metzger, T. G. Birdsall and A. B. Baggeroer, "A test of basin-scale acoustic thermometry using a large-aperture vertical array at 3250-km range in the eastern North Pacific Ocean," *The Journal of the Acoustical Society of America* **105**, 3185-3201 (1999).
- <sup>3</sup> W. T. Wood, W. S. Holbrook, M. K. Sen and P. L. Stoffa, "Full waveform inversion of reflection seismic data for ocean temperature profiles," *Geophysical Research Letters* **35**, L04608 (2008).
- <sup>4</sup> X.-H. Huang, H.-B. Song, L. M. Pinheiro and Y. Bai, "Ocean temperature and salinity distributions inverted from combined reflection seismic and xbt data," *Chinese Journal of Geophysics* **54**, 307-314 (2011).
- <sup>5</sup> B. Ruddick, H. Song, C. Dong and L. Pinheiro, "Water column seismic images as maps of temperature gradient," *Oceanography* **22**, 192-205 (2009).
- <sup>6</sup> B. Biescas, B. R. Ruddick, M. R. Nedimovic, V. Sallarès, G. Bornstein and J. F. Mojica, "Recovery of temperature, salinity, and potential density from ocean reflectivity," *Journal of Geophysical Research: Oceans* **119**, 3171-3184 (2014).

- <sup>7</sup> V. Sallarès, B. Biescas, G. Buffett, R. Carbonell, J. J. Dañobeitia and J. L. Pelegrí, "Relative contribution of temperature and salinity to ocean acoustic reflectivity," *Geophysical Research Letters* **36**, L00D06 (2009).
- <sup>8</sup> D. J. Matthews, *Tables of the velocity of sound in pure water and sea water for use in echo-sounding and sound-ranging*. (Hydrographic Department, British Admiralty, London, 1939) pp.52.
- <sup>9</sup> S. Kuwahara, "Velocity of Sound in Sea Water and Calculation of the Velocity for Use in Sonic Sounding," *Hydrographic Review* **16**, 123-140 (1939).
- <sup>10</sup> C. T. Chen and F. J. Millero, "Speed of sound in seawater at high pressures," *The Journal of the Acoustical Society of America* **62**, 1129-1135 (1977).
- <sup>11</sup> B. D. Dushaw, P. F. Worcester, B. D. Cornuelle and B. M. Howe, "On equations for the speed of sound in seawater," *The Journal of the Acoustical Society of America* **93**, 255-275 (1993).
- <sup>12</sup> V. A. Del Grosso, "New equation for the speed of sound in natural waters (with comparisons to other equations)," *The Journal of the Acoustical Society of America* **56**, 1084-1091 (1974).
- <sup>13</sup> K. V. Mackenzie, "Nine-term equation for sound speed in the oceans," *The Journal of the Acoustical Society of America* **70**, 807-812 (1981).
- <sup>14</sup> A. B. Coppens, "Simple equations for the speed of sound in Neptunian waters," *The Journal of the Acoustical Society of America* **69**, 862-863 (1981).
- <sup>15</sup> N. P. Fofonoff and R. C. Millard, *Algorithms for computation of fundamental properties of seawater*. (Unesco, Paris, France, 1983) pp.53.
- <sup>16</sup> M. Knudsen, *Hydrographic tables*. (G.E.C. Gad, Copenhagen, 1901) pp.66.
- <sup>17</sup> C. Forch, M. Knudsen and S. P. L. Sorensen, *Reports on the constant provisions for the planning of hydrographic tables* (in German, Bianco Lunos Bogtr, København, 1902) pp.151.
- <sup>18</sup> J. P. Jacobsen, "A graphical method to determine the mixing coefficients in the sea," (in German) *Gerlands Beiträge zur Geophysik* **16**, 404-412 (1927).
- <sup>19</sup> N. P. Fofonoff, "Physical properties of seawater: A new salinity scale and equation of state for seawater," *Journal of Geophysical Research: Oceans* **90**, 3332-3342 (1985).
- <sup>20</sup> F. J. Millero and A. Poisson, "International one-atmosphere equation of state of seawater," *Deep Sea Research Part A. Oceanographic Research Papers* **28**, 625-629 (1981).
- <sup>21</sup> F. J. Millero, A. Gonzales and G. K. Ward, "The density of seawater solutions at one atmosphere as a function of temperature and salinity," *Journal of Marine Research* **34**, 61-93 (1976).
- <sup>22</sup> A. Poisson, C. Brunet and J. C. Brun-Cottan, "Density of standard seawater solutions at atmospheric pressure," *Deep Sea Research Part A. Oceanographic Research Papers* **27**, 1013-1028 (1980).
- <sup>23</sup> R. E. Sheriff and L. P. Geldart, *Exploration seismology*, 2nd ed. (Cambridge university press, New York, 1995) pp.628.
- <sup>24</sup> S. Lancaster and D. Whitcombe, "Fast-track 'coloured' inversion," in *SEG Technical Program Expanded Abstracts 2000* (Society of Exploration Geophysicists, USA, 2000), pp. 1572-1575.
- <sup>25</sup> P. Dewangan, G. Sriram, T. Ramprasad, M. V. Ramana and P. Jaiswal, "Fault system and thermal regime in the vicinity of site NGHP-01-10, Krishna–Godavari basin, Bay of Bengal," *Marine and Petroleum Geology* **28**, 1899-1914 (2011).

- <sup>26</sup> S. R. Shetye, A. D. Gouveia, D. Shankar, S. S. C. Shenoi, P. N. Vinayachandran, D. Sundar, G. S. Michael and G. Nampoothiri, "Hydrography and circulation in the western Bay of Bengal during the northeast monsoon," *Journal of Geophysical Research: Oceans* **101**, 14011-14025 (1996).
- <sup>27</sup> S. R. Shetye, A. D. Gouveia, S. S. C. Shenoi, D. Sundar, G. S. Michael and G. Nampoothiri, "The western boundary current of the seasonal subtropical gyre in the Bay of Bengal," *Journal of Geophysical Research: Oceans* **98**, 945-954 (1993).
- <sup>28</sup> G. S. K. Wong and S. m. Zhu, "Speed of sound in seawater as a function of salinity, temperature, and pressure," *The Journal of the Acoustical Society of America* **97**, 1732-1736 (1995).
- <sup>29</sup> O. I. Mamayev, *Temperature-salinity analysis of world ocean waters*. (Elsevier Scientific Publishing Company, The Netherlands, 2010) pp.374.
- <sup>30</sup> P. H. Bigg, "Density of water in SI units over the range 0-40°C," *British Journal of Applied Physics* **18**, 521-537 (1967).
- <sup>31</sup> I. Fer and W. S. Holbrook, "Seismic reflection methods for study of the water column," in *Elements of Physical Oceanography: A Derivative of the Encyclopedia of Ocean Sciences*, edited by J. H. Steele, S. A. Thorpe and K. K. Turekian (Academic Press, London, 2008), pp. 432-441.
- <sup>32</sup> S. Sinha, "Data driven Q-compensation using continuous wavelet transform," in *SEG Technical Program Expanded Abstracts 2014*, edited by B. Birkelo (Society of Exploration Geophysicists, USA, 2014), pp. 5183.
- <sup>33</sup> S. Sinha and K. Sain, "Denoising of seismic data in wavelet transform domain," presented at the 3rd South Asian Geosciences Conference & Exhibition, New Delhi, INDIA, on 11-14 Jan, (2015) pp. 4. on CD ROM
- <sup>34</sup> S. K. Sinha, P. Dewangan and K. Sain, "Estimation of Sea Surface Temperature (SST) Using Marine Seismic Data," *Pure and Applied Geophysics*, 1-12 (2015).
- <sup>35</sup> W. S. Holbrook, I. Fer, R. W. Schmitt, D. Lizarralde, J. M. Klymak, L. C. Helfrich and R. Kubichek, "Estimating Oceanic Turbulence Dissipation from Seismic Images," *Journal of Atmospheric and Oceanic Technology* **30**, 1767-1788 (2013).
- <sup>36</sup> Y. Nakamura, T. Noguchi, T. Tsuji, S. Itoh, H. Niino and T. Matsuoka, "Simultaneous seismic reflection and physical oceanographic observations of oceanic fine structure in the Kuroshio extension front," *Geophysical Research Letters* **33**, L23605 (2006).
- <sup>37</sup> M. Madhupratap, M. Gauns, N. Ramaiah, S. Prasanna Kumar, P. M. Muraleedharan, S. N. de Sousa, S. Sardesai and U. Muraleedharan, "Biogeochemistry of the Bay of Bengal: physical, chemical and primary productivity characteristics of the central and western Bay of Bengal during summer monsoon 2001," *Deep Sea Research Part II: Topical Studies in Oceanography* **50**, 881-896 (2003).
- <sup>38</sup> S. Prasanna Kumar, P. M. Muraleedharan, T. G. Prasad, M. Gauns, N. Ramaiah, S. N. de Souza, S. Sardesai and M. Madhupratap, "Why is the Bay of Bengal less productive during summer monsoon compared to the Arabian Sea?," *Geophysical Research Letters* **29**, 88-81-88-84 (2002).
- <sup>39</sup> H. Achyuthan, R. D. Deshpande, M. S. Rao, B. Kumar, T. Nallathambi, K. Shashi Kumar, R. Ramesh, P. Ramachandran, A. S. Maurya and S. K. Gupta, "Stable isotopes and salinity in the surface waters of the Bay of Bengal: Implications for water dynamics and palaeoclimate," *Marine Chemistry* **149**, 51-62 (2013).

## Figure Captions

Fig. 1. (Color online) Two seismic lines (Line 1 and Line 2) and the nearest CTD location (star) in Krishna-Godavari Basin located in the eastern continental margin of India. The inset shows the zoom out map of the study location. There are two major rivers in the area: Krishna River and Godavari River.

Fig. 2. Temperature and salinity profiles obtained from CTD data. Sea surface location of the CTD is shown in Fig. 1.

Fig. 3. Soundspeed is computed from temperature and salinity data (Fig. 2) using Eq. 1.

Fig. 4. Sensitivity of soundspeed with respect to salinity and temperature is plotted. The grayscale color shows the ratio of  $dc/dT$  to  $dc/dS$  (see Eqs. 2 and 3).

Fig. 5. A workflow to create synthetic seismogram for acoustic reflections using temperature and salinity profiles of CTD data.

Fig. 6. (Color online) Synthetic seismogram shown in black color wiggles is generated using temperature and salinity data from the CTD location which is about 2 km away from the seismic line. The seismic section (part of Line 1) is shown as variable color density plot in the background where peaks are represented in red and troughs in blue. Salinity profile is overlain as green color curve in (a) and temperature profile is shown in (b).

Fig. 7. (Color Online) Synthetic seismograms are shown in black color wiggles overlain on seismic section displayed as variable density color plot. Peaks are shown in red while troughs in blue. (a) Synthetic seismogram is created to highlight salinity effect by smoothing the temperature profile. The salinity effect is more pronounced between 100 and 175 m. (b) The temperature effect is highlighted on the acoustic reflections by smoothing the salinity profile. In deeper depth ( $> 175$  m), the effect of temperature is more pronounced than that of salinity.

Fig. 8. (Color online) Reflectivity data is processed for impedance estimation using seismic ‘colored’ inversion and is plotted in variable density color plot. The curve in black color is relative acoustic impedance (RAI) calculated from CTD data. Impedance in the shallower section is larger than that in the deeper part.

Fig. 9. (Color online) Seismic profiles of Line 1 and Line 2 are shown as variable density color plot. Red colors represent peak while blue colors represent trough. Time to depth conversion is performed using soundspeed estimation from CTD data.

Fig. 10. (Color online) This is to show seismic tie between Line 1 and Line 2 (Fig. 1). It is a very good correlation for 2D seismic lines considering high frequency content of the data and feathering of hydrophone cables during acquisition.

Fig. 11. (Color online) This is impedance inversion section of Line 2. The data was processed using seismic ‘colored’ inversion plugin available in Opendtect seismic data processing software. Relative acoustic impedance layers show thermohaline structures within water column. The dashed line approximation of the dipping high impedance layer has  $0.35^\circ$  dip in the SE direction.

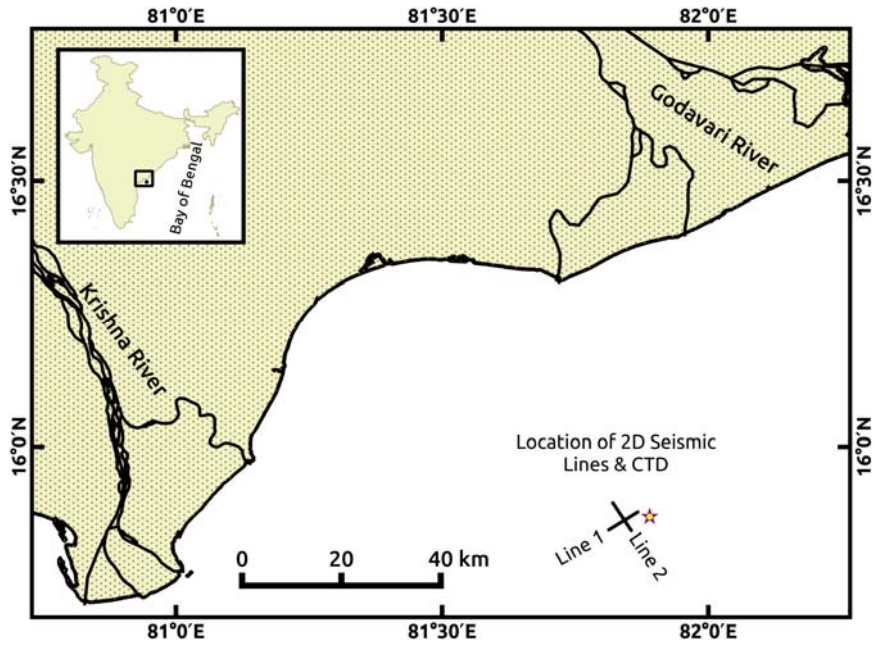


Fig. 1. (Color online) Two seismic lines (Line 1 and Line 2) and the nearest CTD location (star) in Krishna-Godavari Basin located in the eastern continental margin of India. The inset shows the zoom out map of the study location. There are two major rivers in the area: Krishna River and Godavari River.

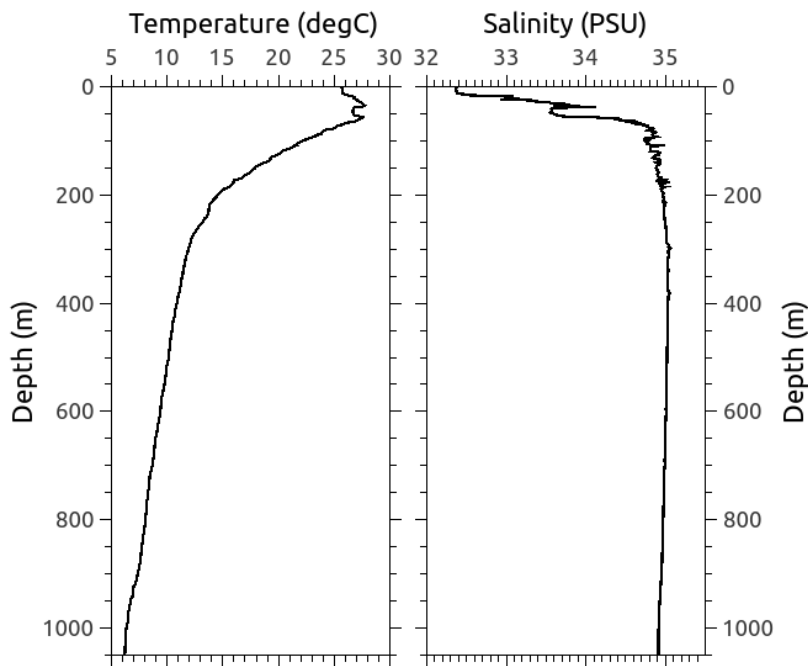


Fig. 2. Temperature and salinity profiles obtained from CTD data. Sea surface location of the CTD is shown in Fig. 1.

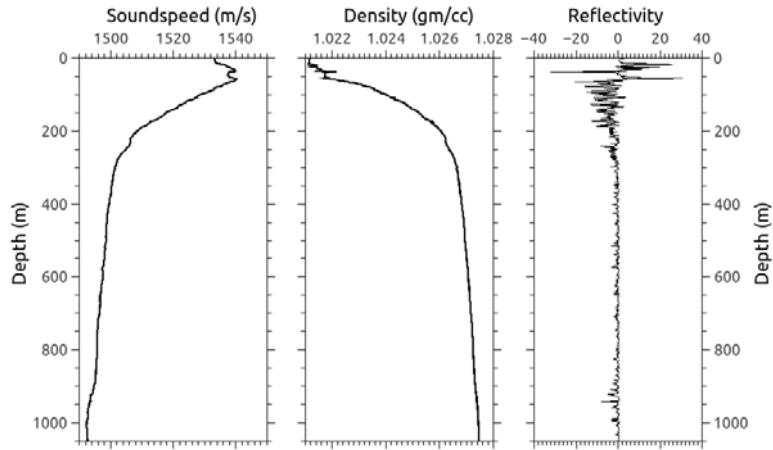


Fig. 3. Soundspeed is computed from temperature and salinity data (Fig. 2) using Eq. 1.

Fig. 4. Sensitivity of soundspeed with respect to salinity and temperature is plotted. The grayscale color shows the ratio of  $dc/dT$  to  $dc/dS$  (see Eqs. 2 and 3).

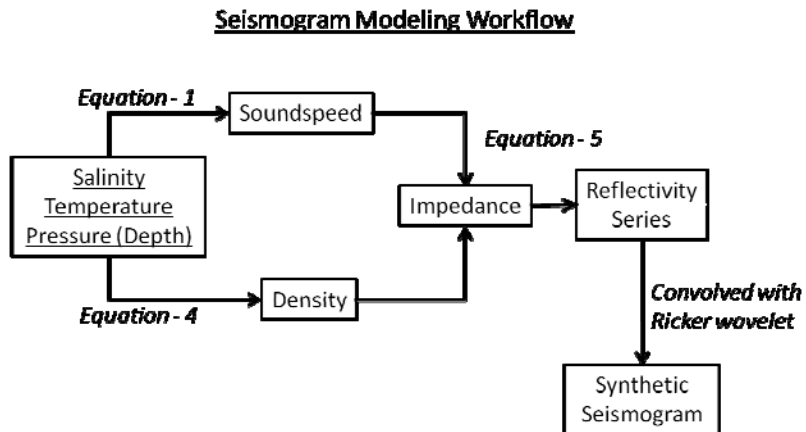


Fig. 5. A workflow to create synthetic seismogram for acoustic reflections using temperature and salinity profiles of CTD data.

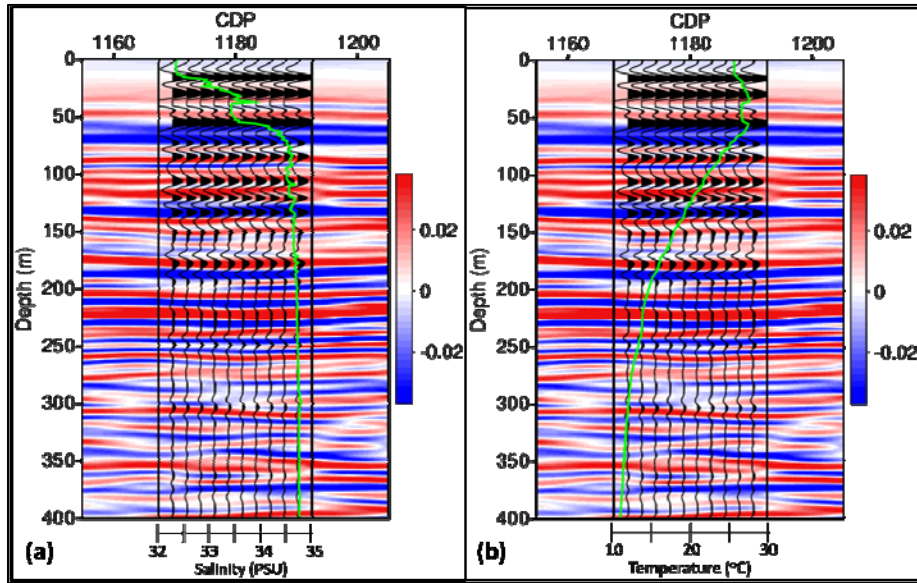


Fig. 6. (Color online) Synthetic seismogram shown in black color wiggles is generated using temperature and salinity data from the CTD location which is about 2 km away from the seismic line. The seismic section (part of Line 1) is shown as variable color density plot in the background where peaks are represented in red and troughs in blue. Salinity profile is overlain as green color curve in (a) and temperature profile is shown in (b).

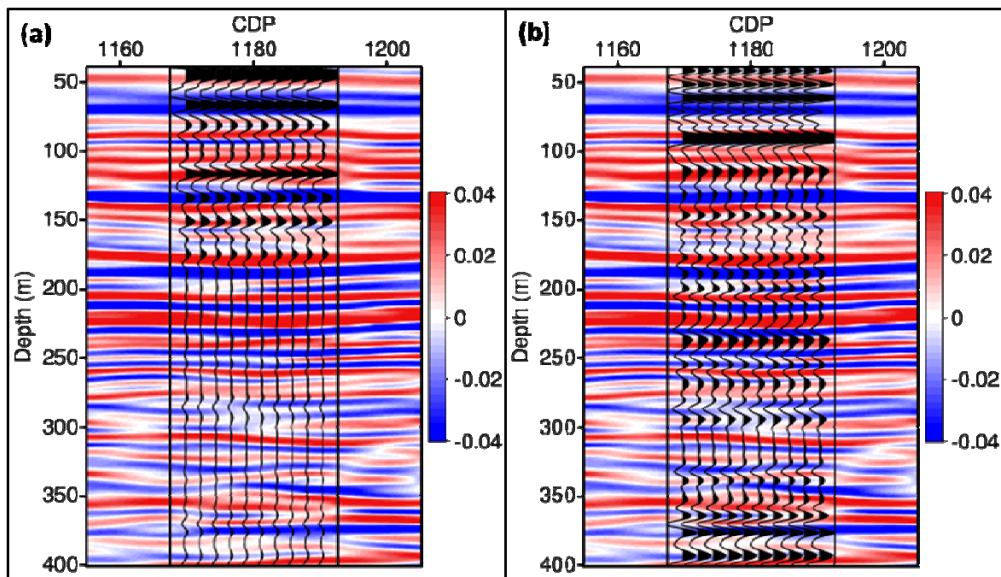


Fig. 7. (Color Online) Synthetic seismograms are shown in black color wiggles overlain on seismic section displayed as variable density color plot. Peaks are shown in red while troughs in blue. (a) Synthetic seismogram is created to highlight salinity effect by smoothing the temperature profile. The salinity effect is more pronounced between 100 and 175 m. (b) The temperature effect is highlighted on the acoustic reflections by smoothing the salinity profile. In deeper depth ( $> 175$  m), the effect of temperature is more pronounced than that of salinity.



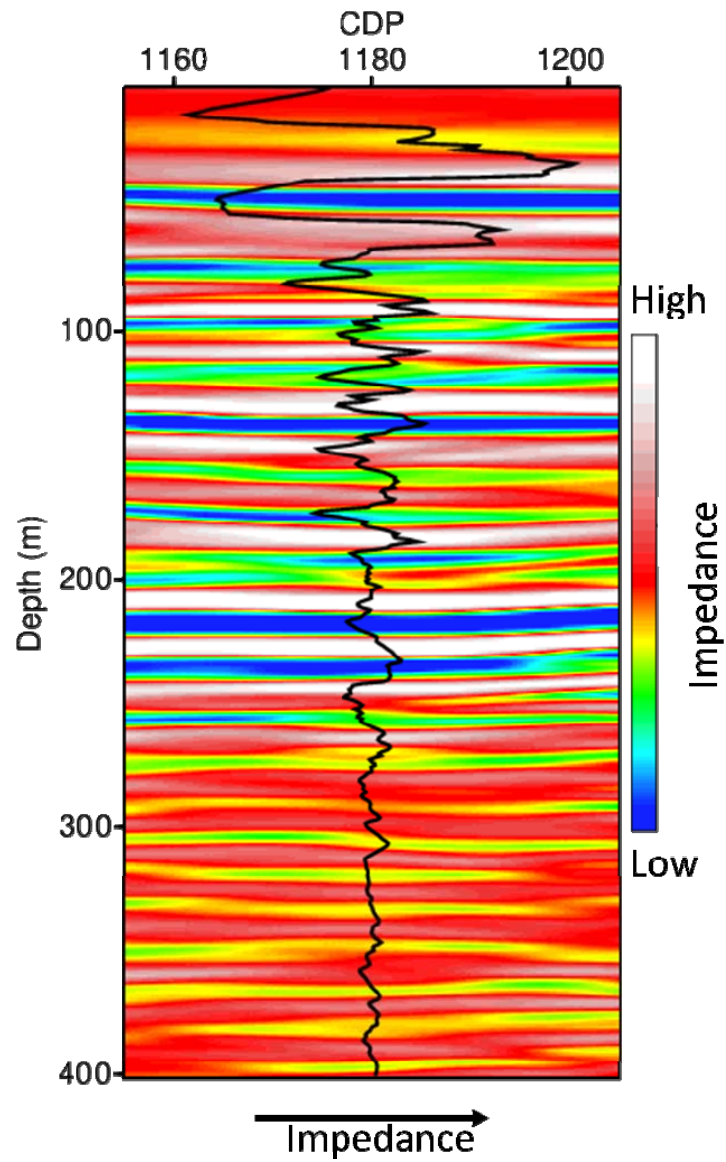


Fig. 8. (Color online) Reflectivity data is processed for impedance estimation using seismic ‘colored’ inversion and is plotted in variable density color plot. The curve in black color is relative acoustic impedance (RAI) calculated from CTD data. Impedance in the shallower section is larger than that in the deeper part.

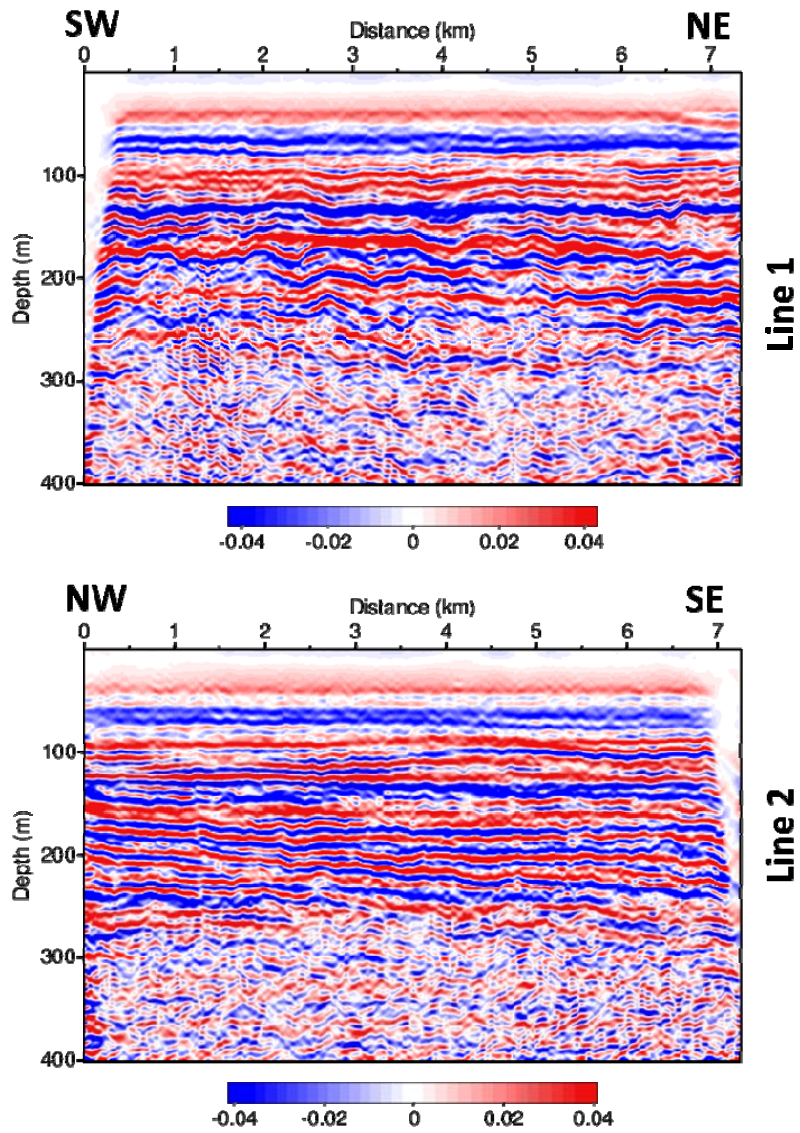


Fig. 9. (Color online) Seismic profiles of Line 1 and Line 2 are shown as variable density color plot. Red colors represent peak while blue colors represent trough. Time to depth conversion is performed using soundspeed estimation from CTD data.

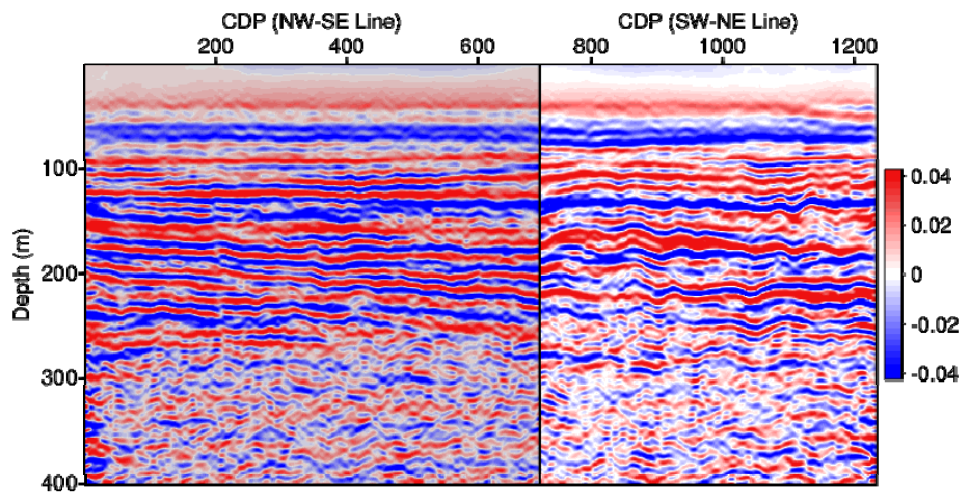


Fig. 10. (Color online) This is to show seismic tie between Line 1 and Line 2 (Fig. 1). It is a very good correlation for 2D seismic lines considering high frequency content of the data and feathering of hydrophone cables during acquisition.

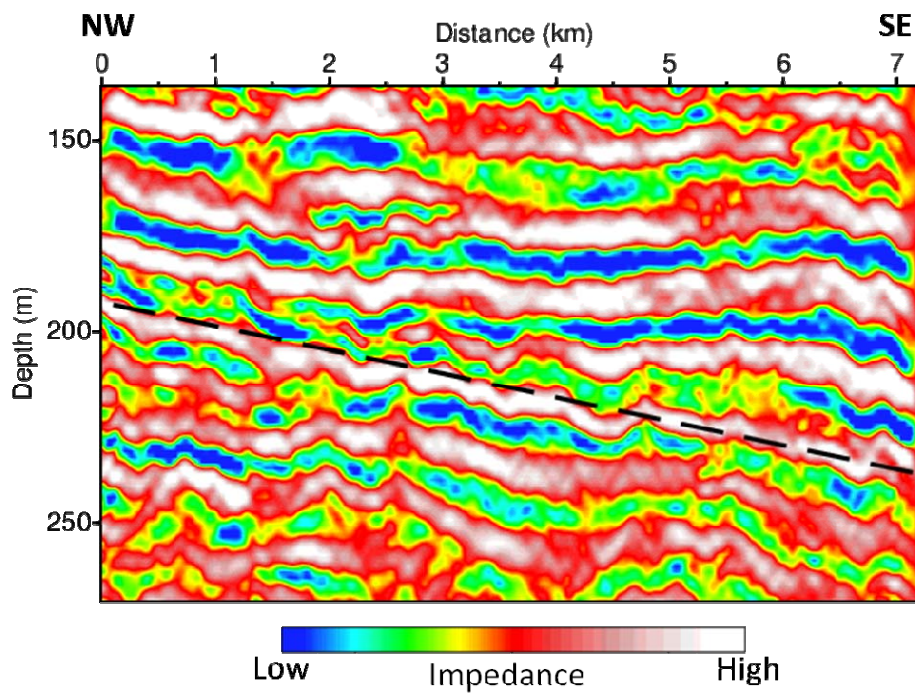


Fig. 11. (Color online) This is impedance inversion section of Line 2. The data was processed using seismic ‘colored’ inversion plugin available in OpendTect seismic data processing software. Relative acoustic impedance layers show thermohaline structures within water column. The dashed line approximation of the dipping high impedance layer has  $0.35^\circ$  dip in the SE direction.